Mon. Not. R. Astron. Soc. **397,** 534–547 (2009) doi:10.1111/j.1365-2966.2009.14962.x

Two-phase galaxy formation

M. Cook,[1,2]★ A. Lapi[1,3,4] and G. L. Granato[2,4]

[1]*Astrophysics Sector, SISSA/ISAS, Via Beirut 2-4, I-34014 Trieste, Italy*
[2]*INAF, Osservatorio Astronomico di Padova, Vicolo dell' Osservatorio 5, I-35122 Padova, Italy*
[3]*Department of Physics, Univ. di Roma 'Tor Vergata', Via della Ricerca Scientifica 1, I-00133 Rome, Italy*
[4]*INAF, Osservatorio Astronomico di Trieste, Via G.B. Tiepolo 11, I-34131 Trieste, Italy*

Accepted 2009 April 22. Received 2009 April 22; in original form 2008 October 24

ABSTRACT

We propose and test a scenario for the assembly and evolution of luminous matter in galaxies which substantially differs from that adopted by other semi-analytic models. As for the dark matter, we follow the detailed evolution of haloes within the canonical Λ cold dark matter cosmology using standard Monte Carlo methods. However, when overlaying prescriptions for baryon evolution, we take into account an effect pointed out in the past few years by a number of studies mostly based on intensive *N*-body simulations, namely that typical halo growth occurs in two phases: an early, fast collapse phase featuring several major merger events, followed by a late, quiescent accretion on to the halo outskirts. We propose that the two modes of halo growth drive two distinct modes for the evolution of baryonic matter, favouring the development of the spheroidal and disc components of galaxies, respectively. We test this idea using the semi-analytic technique. Our galaxy formation model envisages an early coevolution of spheroids and the central supermassive black holes, already tested in our previous works, followed by a relatively quiescent growth of discs around the preformed spheroids. In this exploratory study, we couple our model with the spectrophotometric code GRASIL, and compare our results on several properties of the local galaxy population with observations, finding an encouraging agreement.

Key words: galaxies: evolution – galaxies: formation – cosmology: theory – dark matter.

1 INTRODUCTION

A fundamental issue when modelling the evolution of galaxies in a cosmological context is that the majority of the processes driving baryonic evolution [such as star formation, various feedback mechanisms, accretion on to supermassive black holes (BHs)] operate or originate on scales well below the resolution of any feasible simulation in a cosmic box. Moreover, these processes are highly non-linear, poorly understood from a physical point of view and approximated by means of simplified, often phenomenological, and thus uncertain subgrid prescriptions. Unfortunately, yet unsurprisingly, a number of studies have clearly demonstrated that the results of these models are heavily affected by different choices for such prescriptions (e.g. Benson et al. 2003; Di Matteo, Springel & Hernquist 2005) or for parameter values (e.g. Zavala, Okamoto & Frenk 2008).

Thus extensive comparisons between different scenarios and data are generally conducted by means of semi-analytic modelling (SAM) for baryons, often grafted on to gravity-only simulations for the dark matter (DM) evolution. By definition of SAMs, the general behaviour of the system is outlined a priori, and then translated into a set of (somewhat) physically grounded analytical recipes – suitable for numerical computation over cosmological timescales – for the processes which are *thought* to be more relevant to galaxy formation and evolution.

Although SAMs should not be viewed as complete first principle computations, they provide a convenient and powerful tool to test an assumed galaxy formation scenario (i.e. the general behaviour and the adopted recipes) against existing data and to make predictions on future observations.

In general, SAMs (e.g. Cole et al. 2000; Hatton et al. 2003; Baugh et al. 2005; Cattaneo et al. 2005, 2006; Bower et al. 2006; Croton et al. 2006; Khochfar & Silk 2006; Monaco, Fontanot & Taffoni 2007; Somerville et al. 2008), apart from relatively minor variations, are constructed around two main assumptions: (i) the initial outcome of gas cooling within DM haloes is, at any cosmic epoch, the development of a rotationally supported disc (since Silk 1977; Rees & Ostriker 1977; White & Rees 1978); these discs usually undergo mild to moderate star formation activity, unless extreme choices for the scaling of star formation efficiency with galaxy properties are done; (ii) the most natural driver of episodes

★E-mail: cook@sissa.it

of violent star formation at any redshift is the merging of these gas-rich discs, which in most models also constitutes the main channel for the formation of spheroids, and in particular of large ellipticals (since Cole 1991).

As a result of this disc-merger-driven framework, baryons tend to follow the hierarchical behaviour of DM haloes, and there is no inherent relationship between the morphology and the star formation history of galaxies. This is in sharp contrast with the basic observational fact that low-mass galaxies tend to be disc-dominated, gas-rich, blue and actively star forming, whilst more massive galaxies tend to be red, gas-poor, quiescent and dominated by a spheroidal component mainly comprising old stars.

Due to these features, SAMs built around the two aforementioned assumptions – which from now on will be collectively referred to as 'standard SAMs' – tend to be in tension with several observations (e.g. Somerville et al. 2008), manifested by the poor performances they had in anticipating observational breakthroughs occurred more recently. For example, it is now well established that baryonic structures undergo the phenomenon referred to as 'cosmic downsizing', whereby massive star-forming systems and associated supermassive BHs shined mostly at high redshift, while smaller objects display longer lasting activity. Clearly, it is challenging to obtain this behaviour from the scheme outlined above; indeed, no model did until relatively recently, and the present situation remains unclear. In the past few years, almost all semi-analytic teams introduced simple recipes of feedback from active galactic nuclei (AGN) in their models, with the specific target of quenching star formation in high-mass galaxies at low redshift. This additional ingredient significantly improves the situation, but does not directly alleviate model difficulties in producing enough massive systems at high z. As a result, at least three state-of-the-art standard SAMs still do not correctly reproduce the downsizing trend in stellar mass, nor the *archaeological downsizing* (Fontanot et al. 2009; see below for more details).

A further example of challenges to models comes from the modest evolution of the cosmic star formation activity above $z \sim 1$ (the so-called Madau plot), strikingly at variance with model predictions (e.g. Cole et al. 1994) generated before the advent of surveys effective in discovering dust-enshrouded star formation at high z (Madau et al. 1996; Madau, Pozzetti & Dickinson 1998). It is fair to note that a fraction, but not all, of the discrepancy was due to the then adopted standard cold dark matter (CDM) cosmology and a lower normalization for the fluctuation spectrum, resulting in significantly more rapid evolution at high redshift than the now favoured ΛCDM.

In addition, even latest and most refined SAMs are seriously challenged by the bright number counts and the high-redshift peak of z-distribution for submillimetre (submm) galaxies. For instance, Baugh et al. (2005) showed that the only way to reproduce the statistic of submm sources, usually considered the precursor of local ellipticals, in the context of their standard SAM is to adopt an extremely top-heavy initial mass function (IMF) during galaxy-merger-induced starbursts. However, their model predicts masses of submm sources likely too low by more than one order of magnitude (Swinbank et al. 2008), and still shows discrepancies with observed trends of α/Fe in local ellipticals (Nagashima et al. 2005).

Without doubt, the field of galaxy formation is *led* by observations. Indeed, physical processes have been continuously added to SAMs, or existing ones have been substantially revised by SAM developers in order to face serious mismatches between model outputs and new data sets. Besides many relatively minor but subtle details, major examples comprise a treatment of the growth of supermassive BHs in galaxy centres and of the ensuing energetic feedback from nuclear activity (Granato et al. 2004, hereafter G04;[1] Bower et al. 2006; Croton et al. 2006; Monaco et al. 2007; Somerville et al. 2008),[2] the effects of 'cold' versus 'hot' accretion flows on to DM haloes, as suggested by Dekel & Birnboim (2006) and implemented in a full SAM by Cattaneo et al. (2006; see also Somerville et al. 2008), or an extremely top-heavy flat IMF in merger-driven bursts (Baugh et al. 2005). These examples show that the complexity and degrees of freedom of standard SAMs have been steadily increased by modellers in order to improve the agreement with the data, but despite these efforts several points of tension still remain (see Monaco et al. 2007).

Within this paper, we follow a significantly different approach and submit a novel scenario for galaxy formation, modifying the very basic assumptions of standard SAMs that, according to us, are the origin of their tensions with observations. Our scenario envisages that the fundamental dichotomy between the spheroid and disc components in galaxies reflects two dominating modes for the assembly of visible matter, feasibly being ultimately driven by two dominating modes governing the growth of DM haloes (see below). For typical L^* galaxy haloes, $z \gtrsim 2$ corresponds to an era dominated by violent merging episodes, leading to huge bursts of star formation and to the observed coevolution of spheroids with hosted central supermassive BHs; $z \lesssim 2$ instead corresponds to an era where the most relevant process is quiescent accretion of matter yielding, under suitable conditions, the formation of discs around pre-existing spheroids.

Many studies in the literature on the chemical and spectrophotometric properties of local galaxy populations (*stellar archaeology*; see Thomas et al. 2005 and references therein; Chiappini, Matteucci & Gratton 1997; Portinari & Chiosi 1999) reached the broad conclusion that galaxies of later type, which are less massive on average, formed their stars at later times and over a longer period (see also Gavazzi et al. 1996). This phenomenon is sometimes referred to as *archaeological downsizing* and is not reproduced by three state-of-the-art SAMs (Fontanot et al. 2009; however, see Kaviraj et al. 2005 for a discussion of colour–magnitude relation in cluster ellipticals as a test for hierarchical models). These conclusions have more recently been confirmed by modern surveys at high redshift, directly showing that the sites of active star formation shift from high-mass galaxies at early times to lower mass systems at later times (*downsizing in time*; Cowie et al. 1996; Guzman et al. 1997; Brinchmann & Ellis 2000; Kodama et al. 2004; Bell et al. 2005; Juneau et al. 2005; Noeske et al. 2007). Further support for two different epochs and formation mechanisms of spheroids and discs comes from the analysis of the colour and structural properties of decomposed galaxy components in the Millennium Galaxy Catalogue (Driver et al. 2006).

From the theoretical perspective, recent analysis of high-resolution simulations of individual DM haloes forming in cosmological volumes (Zhao et al. 2003; Diemand, Kuhlen & Madau 2007; Hoffman et al. 2007; Ascasibar & Gottloeber 2008) has provided support for our picture. In these studies, two distinct phases in the growth of DM haloes have been identified: an early, fast collapse featuring a few violent major mergers, and a later calmer phase

[1] In the context of a non-standard SAM focused on the coevolution of quasars and spheroids, of which this paper can be considered an extension, see below.

[2] See also Hatton et al. (2003) and Cattaneo et al. (2007) for the effect of a highly idealized criterion of 'pseudo-AGN feedback', phenomenologically inspired by the Magorrian et al. (1998) relationship.

including many minor mergers and smooth accretion. During the early collapse, a substantial mass is gathered through major mergers, which effectively reconfigure the gravitational potential wells and cause the collisionless DM particles to undergo dynamical relaxation and isotropization (Lapi & Cavaliere 2009); therefrom, the system emerges with a definite structure for the inner density and gravitational potential (Lu et al. 2006). During the later quiescent phase, moderate amounts of mass are slowly accreted mainly on to the halo outskirts, little affecting the inner structure and potential, but quiescently rescaling the overall mass upwards. Mo & Mao (2004) qualitatively suggested that this two-phase formation of DM haloes may be at the origin of the disc–spheroid dichotomy, alleviating several problems of the standard SAMs. Here we take up this general idea, and construct a full semi-analytic model capable at making quantitative predictions to be compared with present and future observations. We explicitly point out that the backbone for the cosmological growth of DM haloes is broadly the same as that adopted by all other SAMs. The novelty is in the fact that we identify the transition between the two phases, and we assume that the main processes driving the evolution of luminous matter are strongly linked to the two different modes of DM assembly.

Our model constitutes a natural extension to include disc formation at low z, of the antihierarchical baryon collapse (ABC) scenario (G04; Silva et al. 2005; Granato et al. 2006; Lapi et al. 2006; Mao et al. 2007; Lapi et al. 2008) that was focused on the high-redshift coevolution between spheroidal galaxies and hosted supermassive BHs. This has been extremely successful in reproducing a wealth of observations, including statistics of submm galaxies, properties of local elliptical galaxies, the results of deep K-band surveys, the estimated local mass function of supermassive BH and statistics of high-redshift quasars [quasi-stellar objects (QSOs)]. These results are essentially inherited by the model presented here.

In summary, motivated by the successes of the high-redshift ABC framework and the compelling theoretical and observational evidence in support of a two-phase galaxy formation scenario, we have developed a framework linking high- and low-redshift processes in order to generate the observed dichotomy between early- and late-type galaxies. The plan of this paper is as follows: we describe in detail the two-phase DM treatment in Section 2; in Section 3, we describe the modelling of the baryonic matter evolution for the spheroid and disc components; we present our results in Section 4 and finally we summarize and discuss our findings in Section 5.

Throughout this paper we adopt the standard ΛCDM concordance cosmology, as constrained by *Wilkinson Microwave Anisotropy Probe* 5-year data (Spergel et al. 2007). Specifically, we adopt a flat cosmology with density parameters $\Omega_{\rm M} = 0.27$ and $\Omega_\Lambda = 0.73$, and a Hubble constant $H_0 = 70\,{\rm km\,s^{-1}\,Mpc^{-1}}$.

2 DARK MATTER SECTOR

In this work, we compute the mass growth histories of DM haloes using a binary merger tree with accretion based on the extended Press & Schechter formalism (see Lacey & Cole 1993); specifically, we rely on the algorithm originally developed by Cole et al. (2000), and recently improved by Parkinson, Cole & Helly (2008) to reproduce the outcomes of N-body simulations.

The algorithm starts from the expression for the mass fraction of a halo with mass M_2 at redshift z_2 that was contained within a progenitor halo of mass $M_1 < M_2$ at $z_1 > z_2$:

$$f = \frac{\Delta\delta_{\rm c}}{\sqrt{2\pi\,(\Delta\sigma^2)^3}}\,{\rm e}^{-(\Delta\delta_{\rm c})^2/2\,\Delta\sigma^2}\,\left|\frac{{\rm d}\sigma^2}{{\rm d}M}\right|_{M=M_1}, \tag{1}$$

where $\Delta\delta_{\rm c} = \delta_{\rm c}(z_1) - \delta_{\rm c}(z_2)$ is the difference between the linear thresholds for collapse at redshifts z_1 and z_2, while $\Delta\sigma^2 = \sigma^2(M_1) - \sigma^2(M_2)$ is the difference between the variances of the linear density fluctuations extrapolated at $z = 0$ in spheres containing masses M_1 and M_2.

Taking the limit of the above equation as $z_1 \to z_2$, one finds the merger rate as

$$\frac{{\rm d}f}{{\rm d}z} = \frac{1}{\sqrt{2\pi\,(\Delta\sigma^2)^3}}\,\left|\frac{{\rm d}\delta_{\rm c}}{{\rm d}z}\right|\,\left|\frac{{\rm d}\sigma^2}{{\rm d}M}\right|_{M=M_1}; \tag{2}$$

now one can easily work out the distribution for the number of haloes with mass M_1 into which a halo with mass M_2 splits during a step ${\rm d}z$ up in redshift:

$$\frac{{\rm d}N}{{\rm d}M_1} = \frac{{\rm d}f}{{\rm d}z}\,\frac{M_2}{M_1}\,{\rm d}z. \tag{3}$$

Then, given a mass resolution $M_{\rm res}$ one may define the mean number of progenitors with masses M_1 between $M_{\rm res}$ and $M_2/2$:

$$P = \int_{M_{\rm res}}^{M_2/2}\frac{{\rm d}N}{{\rm d}M_1}\,{\rm d}M_1, \tag{4}$$

and the fraction of mass of the final object in progenitors below the resolution limit:

$$F = \int_0^{M_{\rm res}}\frac{{\rm d}N}{{\rm d}M_1}\,\frac{M_1}{M_2}\,{\rm d}M_1. \tag{5}$$

In fact, in constructing the above quantities we have replaced

$$\frac{{\rm d}N}{{\rm d}M_1} \longrightarrow \frac{{\rm d}N}{{\rm d}M_1}\,G(\sigma_1/\sigma_2, \delta_2/\sigma_2), \tag{6}$$

where $G(\sigma_1/\sigma_2, \delta_2/\sigma_2)$ is a perturbing function given by Parkinson et al. (2008), tuned to bring the Monte Carlo merger histories in close agreement with the outcomes of state-of-the-art numerical simulations.

Given this theoretical framework, the merger tree algorithm is straightforward: select a mass M_2 and redshift z for the final halo; define an interval in redshift ${\rm d}z$ such that $P \ll 1$ to ensure that the halo is unlikely to have more than two progenitors at $z + {\rm d}z$; generate a uniform deviate random number R between 0 and 1; if $R > P$ the halo does not split over this interval, and simply reduces its mass to $M_2(1 - F)$ to account for subresolution accretion; if $R \leq P$ generates a random value of M_1 between $M_{\rm res}$ and $M_2/2$ consistent with the distribution given by equation (1) to produce two new haloes with masses M_1 and $M_2(1 - F) - M_1$, repeat this process on each new halo at successive redshift intervals to build the overall merging tree.

In our implementation of the algorithm, we use an adaptive step size Δz such that P remains at a value significantly below unity, and then post-process the tree by sampling it over convenient redshift intervals. In addition, we take the resolution mass $M_{\rm res}(z)$ as the one corresponding to a virial temperature of 10^4 K, above which atomic gas cooling allows baryonic structures to condense.

As an input of the algorithm, we use the Bardeen et al. (1986) power spectrum of density fluctuations with correction for baryons (Sugiyama 1995), normalized so as to yield a mass variance $\sigma_8 \approx 0.8$ on a scale of $8\,h^{-1}$ Mpc. As an output, we obtain many realizations (up to several thousands within conceivable computational times) of the merger tree for a given present mass M_0 at $z = 0$; each realization lists all the progenitors of M_0 at different redshifts and describes how and when these merge together. We generate trees for masses M_0 spanning the range from 10^9 to $10^{14}\,{\rm M}_\odot$ in logarithmic increments, and follow the related merging histories down to the resolution mass.

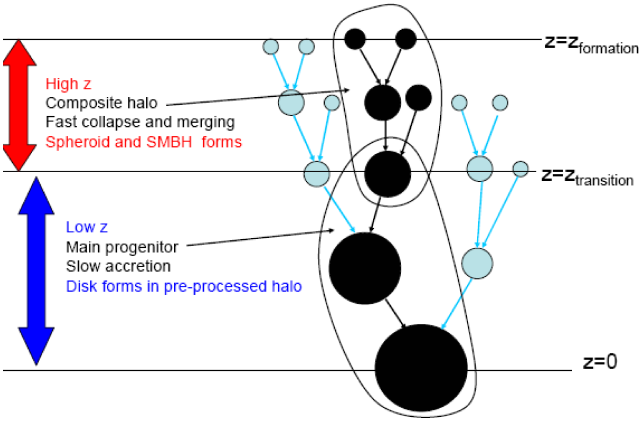

Figure 1. A schematic of the two-phase evolution of DM haloes and associated modes of galaxy formation.

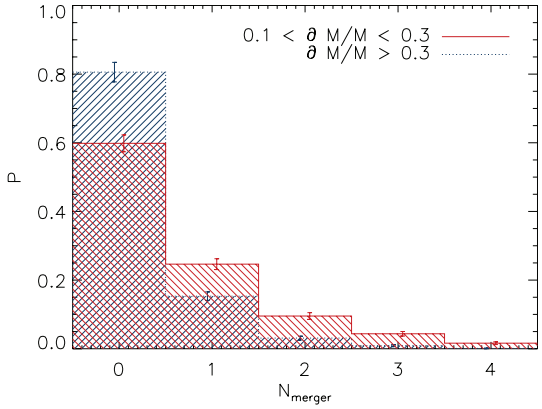

Figure 2. Probability distribution for the number of mergers undergone by DM haloes during the slow accretion phase (results over 1000 realizations); various line styles refer to different ranges for the relative mass addition $\Delta M/M$. In general, major mergers between haloes are very rare events during the slow phase.

We find that the halo growth along a given evolutionary track occurs in two distinct phases: an early violent collapse where rapid growth is enforced by major mergers among several massive clumps; and a late period of gentle mass addition through calmer accretion (see Fig. 1) extending down to the present time. A similar behaviour has been pointed out in a number of recent numerical simulations (Wechsler et al. 2002; Zhao et al. 2003; Diemand et al. 2007; Hoffman et al. 2007; Ascasibar & Gottloeber 2008), and has been analysed in semi-analytic studies of Monte Carlo merging trees to explore the origin of the structural properties of DM haloes (see Lu et al. 2006; Li et al. 2007; Lapi & Cavaliere 2009).

In our view, these different evolutionary phases of DM halo growth should significantly affect the main physical processes regulating the evolution of the baryonic matter within them; in particular, we envisage the violent early collapse phase to be associated with the formation of the spheroid and hosted supermassive BH, while the gentle late phase to be favourable for the stable growth of galaxy disc around the pre-existing spheroid–BH structure.

As to the halo spatial structure we assume the standard NFW (Navarro, Frenk & White 1997) density profile

$$\frac{\rho(r)}{\rho_{\rm c}} = \frac{\Delta_{\rm vir}\, c^2\, g(c)}{3\,(r/r_{\rm vir})\,(1 + c\,r/r_{\rm vir})^2}, \qquad (7)$$

where $\rho_{\rm c}$ is the critical density, $g(c) \equiv [\log(1+c) - c/(1+c)]^{-1}$ is a weak function of the 'concentration' parameter c and $\Delta_{\rm vir} \approx 18\pi^2 + 82\,[\Omega_{\rm M}(z) - 1] - 39\,[\Omega_{\rm M}(z) - 1]^2$ is the non-linear collapse threshold in terms of the evolved matter density parameter $\Omega_{\rm M}(z) = \Omega_{\rm M}(1+z)^3/[\Omega_{\rm M}(1+z)^3 + \Omega_\Lambda]$. In fact, N-body experiments (Taylor & Navarro 2001; Zhao et al. 2003; Diemand et al. 2007; Hoffmann et al. 2007; Ascasibar & Gottloeber 2008) show that the NFW profile is established during the early, fast collapse phase, with concentration parameter $c_{\rm t} \simeq 4$ for $z \gtrsim z_{\rm t}$; in the slow accretion phase for $z \lesssim z_{\rm t}$, the DM halo potential well retains its shape and r_s stays put while the overall size $r_{\rm vir}$ of the system increases, to the effect of rising the concentration parameter, see below.

Equipped with these notions, we effectively trace the redshift evolution in the tree of a DM halo mass M_z with present value M_0 as follows (see Fig. 1). First of all, we compute the concentration c_0 of the mass M_0 according to the prescription by Macciò et al. (2007):

$$\log c_0 = 1.071 - 0.098\,\left[\log\left(\frac{M_0}{{\rm M}_\odot}\right) - 12\right]; \qquad (8)$$

we stress that our computation neglects the scatter of c_0 at fixed mass, and any dependence of c_0 itself on the details of the merging history (see Wechsler et al. 2002; Zhao et al. 2003). In addition, for the sake of simplicity we disregard the influence of the baryons on the halo structure in terms of adiabatic contractions or expansions (see Blumenthal et al. 1986; Gnedin et al. 2004).

Then, during the late, slow accretion phase we take M_z as the mass of the main progenitor, i.e. we follow only the main branch of the merger tree. This is achieved by starting at $z = 0$ and working towards higher redshifts, taking the most massive halo at each splitting (merger) event. We neglect the baryonic processes (in particular star formation) occurring in the other branches of the tree; in other words, we make the approximation that when matter in the minor branches of the tree joins the main progenitor it is still pristine, unevolved by baryonic processes and thus mainly in the form of a gaseous medium with primordial metallicity. This is conceivable since these haloes have masses close to the cooling mass, and thus have just grown from below this threshold; we expect the star formation efficiency to be relatively low there, since supernova (SN) feedback would be most effective in ejecting gas from such shallow potential wells; such small haloes are likely to contain small galaxies that would not significantly alter the properties of the galaxy hosted by the main progenitor if they happened to merge with it.

For a quantitative analysis, we compute and illustrate in Figs 2 and 3 the properties of mergers undergone by DM haloes along their growth history during the slow accretion phase. We find that DM haloes grow predominantly through small accretion events and that the majority of our haloes (about 80 per cent) do not undergo a substantial merger event; we recall that conventionally a major merger is defined as the one in which the added mass exceeds that of the merging units by 1/3 or more, i.e. $\Delta M/M > 1/3$ (see Lacey & Cole 1993). Note, however, that a minority of haloes (20 per cent or so) do undergo a major merger event; plainly, within these systems the growth of stable galaxy discs can be temporarily interrupted. In addition, we note that the number of major mergers during the slow accretion phase is closely independent of halo mass; thus the average major merger rate is higher for more massive haloes, which have more recently made their transition into the slow accretion phase.

We compute the concentration c_z associated with the mass M_z after Zhao et al. (2003) using

$$\frac{[\log(1+c_z) - c_z/(1+c_z)]\,c_z^{-3\alpha}}{[\log(1+c_0) - c_0/(1+c_0)]\,c_0^{-3\alpha}} = \left(\frac{H_z}{H_0}\right)^{2\alpha}\left(\frac{M_z}{M_0}\right)^{1-\alpha}, \qquad (9)$$

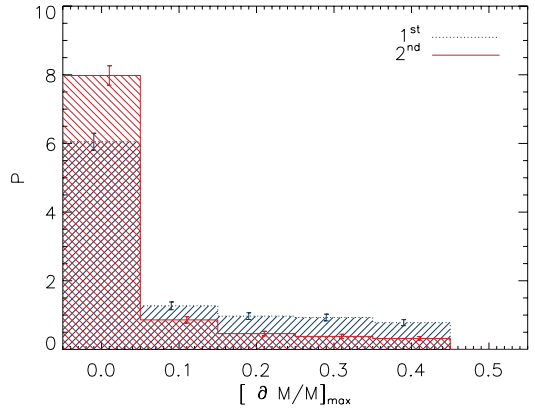

Figure 3. Probability distribution for the relative mass addition to haloes during the slow accretion phase (results over 1000 realizations); various line styles refer to the largest and the second largest value of $\Delta M/M$ in the tree during the slow accretion phase. In general, the dominant mechanism for growing haloes in the slow phase is the accretion of small lumps.

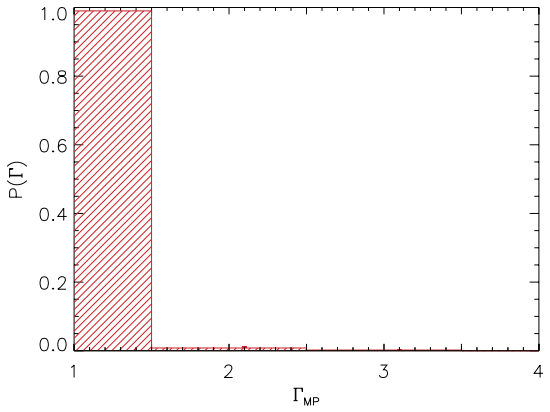

Figure 4. Probability distribution for the mass rank of the main progenitor in the merger tree at z_t. In general, the main progenitor is actually the most massive halo at the transition.

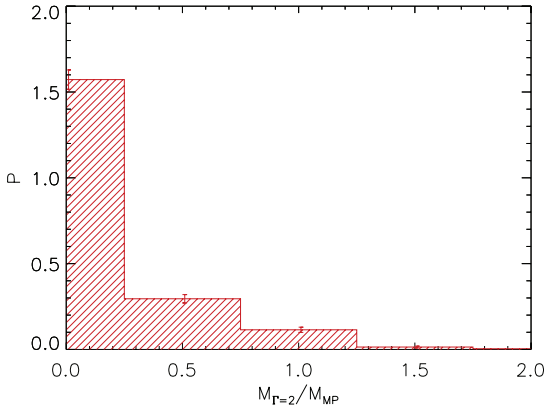

Figure 5. Probability distribution for the mass ratio between the main progenitor and the most massive of all other haloes in the merger tree at z_t; in general, all the other haloes are significantly less massive than the main progenitor.

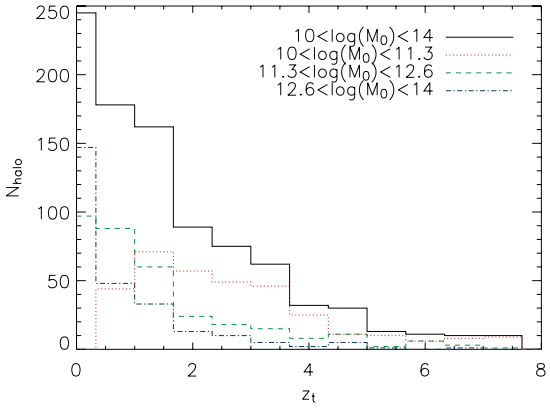

Figure 6. Probability distribution for the transition redshifts (results over 1000 realizations); various line styles are for different ranges of present halo mass M_0. The distributions of z_t are roughly lognormal with a low-redshift peak and a rather extended tail at high z. Note that lower mass haloes have a higher z_t on the average.

where $\alpha = 0.48$ (0.64) in the slow (fast) phase is a fitting parameter derived from N-body simulations and $H_z = H_0\,[\Omega_M(1+z)^3 + \Omega_\Lambda]^{1/2}$ is the evolved 'Hubble constant'; a less accurate but simpler approximation of the expression above in the slow phase reads as $c_z = c_0\,[H_0/H_z]^{1/\eta}$ with $\eta \sim 1$ (see Mo & Mao 2004). Following Zhao et al. (2003), the transition between the slow accretion and the fast major merger phase occurs at the redshift z_t where the concentration c_z decreases below the critical value $c_t = 4$.

In Figs 4 and 5, we illustrate the properties of the merger tree at z_t. First, we note that the main progenitor is generally the most massive halo in the merger tree at z_t; secondly, the ratio between the mass of the main progenitor halo and the second most massive halo is generally very large. These findings show that, during the late slow accretion phase, the relevant evolution of the main progenitor is characterized by minor merger events with low-mass haloes.

It is interesting to note (see Fig. 6) that on average the transition redshift z_t decreases with increasing present-day halo mass. In our scenario, this means that larger haloes have less or no time to develop a substantial disc component, hence massive haloes will tend to host pure spheroids and vice versa, in broad agreement with observations. Incidentally, note that although massive haloes spend the majority (or all) of their lifetimes within the fast collapse phase, the time-scales for baryonic evolution, that are governed by the coevolution of the spheroid and the central supermassive BH, can be much shorter; in fact, these systems typically become 'red and dead' due to QSO feedback at relatively high redshifts, and passively evolve thereafter until the present (see Section 3.1).

At $z > z_t$, during the fast collapse phase, we compute M_z not as the main progenitor mass, but as that of the composite halo made of the overall mass in all the branches of the tree that will contribute to the main progenitor mass at z_t. Moreover, we consider only haloes whose mass exceeds the critical halo mass for efficient gas cooling, i.e. we consider only haloes where the related virial temperature is above 10^4K.

Quantitatively, this can be justified by comparing the dynamical time for the composite halo with the major merger time-scale. The former is defined as the time-scale for the material to ballistically collapse to its centre:

$$\tau_{\rm coll} = \left(\frac{3\pi}{32\,G\,\bar{\rho}}\right)^{1/2}, \tag{10}$$

in terms of the average density of the composite halo; the latter is defined as the average time-scale for a major merger throughout the duration of the fast collapse phase:

$$\tau_{\rm merge} = \frac{N_{\rm MM}}{\delta t_{\rm fast}}, \tag{11}$$

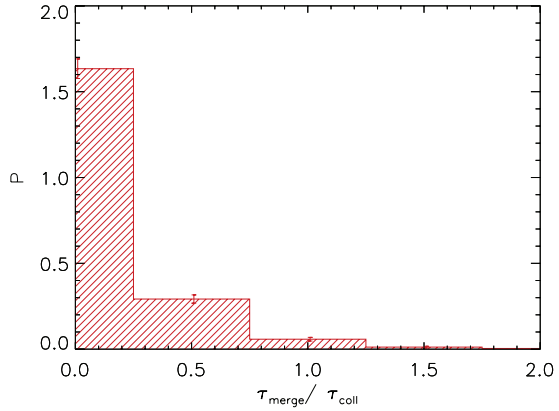

Figure 7. Probability distribution for the ratio between the merging time and the dynamical time of the individual merging units during the early, fast collapse phase (results over 1000 realizations). In general, during the early collapse mergers occur on very short time-scales.

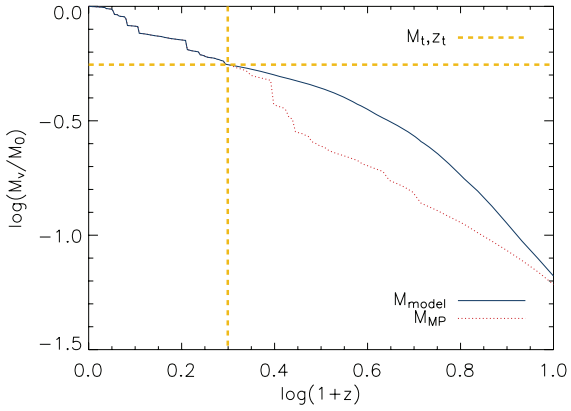

Figure 8. Typical mass accretion history for a Milky Way sized DM halo ($M_0 \approx 5 \times 10^{11}\,\mathrm{M}_\odot$). The transition between slow accretion and fast collapse, that occurs at a redshift $z_t \approx 1$, is highlighted as a dashed line. The halo growth (solid line) follows the main progenitor's one (dot–dashed line) during the late slow accretion phase, and the composite halo (see the text for details) during the early, fast collapse.

where $N_{\rm MM}$ is the number of times the main progenitor undergoes a major merger during the fast collapse phase and $\delta t_{\rm fast}$ is the time lapse the halo spends within it.

Fig. 7 shows that during the fast collapse phase several major merger events occur over time-scales typically shorter than the dynamical time of the composite system, so just following the composite halo is a conceivable approximation.

In Fig. 8, we plot one typical realization of the mass accretion history for a Milky Way sized DM halo, highlighting the transition redshift z_t, the behaviour of the composite halo at $z > z_t$ and of the main progenitor at $z < z_t$.

Finally, we specify the angular momentum of the DM halo in the merger tree as follows. First of all, we recall that the angular momentum J is usually expressed in terms of the dimensionless spin parameter $\lambda \equiv J\,|E|^{1/2}\,G^{-1}\,M^{-5/2}$, where E is the total energy of the halo, N-body experiments have shown that λ does not correlate with halo mass nor with concentration, is nearly independent of the redshift and follows a lognormal distribution with average value 0.04 and scatter 0.5 dex (Bullock et al. 2001; Macciò et al. 2007).

Thus, for each halo we randomly select a value of λ from such a distribution and neglect its evolution (e.g. Barnes & Efstathiou 1987; Kravstov, Klypin & Khokhlov 1997; Vitvitska et al. 2002; Hetznecker & Burkert 2006). We are aware that the latter could impact on the evolution of disc properties, but choose to keep our treatment of this effect as simple as possible, given that to our knowledge a robust modelling has not yet been included into state-of-the-art SAMs; e.g. Somerville et al. (2008) use the spin parameter of the more massive halo at any given merger event.

3 BARYONIC SECTOR

3.1 Modelling the spheroid

The treatment of the baryonic processes in the fast major merger phase follows the recipes adopted by G04 to model the coevolution of spheroids and supermassive BHs, and already exploited by our team in several previous papers (Cirasuolo et al. 2005; Silva et al. 2005; Granato et al. 2006; Lapi et al. 2006; Mao et al. 2007; Lapi et al. 2008). Here, we provide a qualitative summary of the model focusing on its distinctive features, and defer the reader to G04 for all the details.

We recall from Section 2 that during the fast collapse phase, a rapid sequence of major mergers build up a DM halo of mass M_t at the transition redshift z_t; as for baryonic matter, we assume that condensation and cooling processes become effective at a formation redshift $z_f > z_t$ when the mass of the composite halo surpasses a substantial fraction of M_t, namely $M_t/2$ as widely adopted in the literature to define the 'formation epoch' (Lacey & Cole 1993; Kitayama & Suto 1996). The results presented in this paper are almost insensitive to the exact choice for the fraction of M_t adopted in the definition of z_f. Specifically, we have checked that galaxy properties vary less than 10 per cent when the mass fraction is changed between approximately 1/5 and 2/3, due to the strong effects of QSO feedback in terminating the star formation soon after z_f.

After z_f, a mass $M_{\rm inf} \approx f_b\,M_t$ of baryonic matter, in cosmic proportion $f_b \approx 0.17$ with the DMs, is shock heated to the virial temperature by falling into the gravitational potential well. This hot gas, assumed to follow an isothermal distribution, may cool quickly especially in the denser central regions at the rate

$$\dot{M}_{\rm cool} = \frac{M_{\rm inf}}{t_{\rm cool}}, \tag{12}$$

in terms of the local cooling time-scale

$$t_{\rm cool} = \frac{3\,\rho_{\rm gas}\,kT}{2\mu m_p\,\mathcal{C}\,n_{\rm e}^2(r)\,\Lambda(T)}, \tag{13}$$

where $\rho_{\rm gas}$ is the gas density, $n_{\rm e}$ is the electron density, T is the temperature, $\Lambda(T)$ is the cooling function and $\mathcal{C} \sim 5 - 10$ is a parameter describing the clumpiness of the gas.

The cooled gas mass $M_{\rm cold}$, assumed to still follow the DM radial distribution, may form stars directly over the local dynamical time-scale, providing a rate of star formation

$$\psi(t) = \int_0^{r_{\rm vir}} \frac{1}{t_{\rm dyn}(r)}\,\frac{{\rm d}M_{\rm cold}(r,t)}{{\rm d}r}\,{\rm d}r, \tag{14}$$

with

$$t_{\rm dyn} = \left[\frac{3\pi}{32\,G\rho(r)}\right]^{1/2}. \tag{15}$$

This is conceivable during this evolutionary stage since the ongoing major mergers continuously reshuffle the gravitational potential, enforcing dynamical relaxation and orbit isotropization of the collisionless DM and stellar components (Lapi & Cavaliere 2009). We

recall that usually SAMs assume instead that the first result of gas cooling is the formation of rotationally supported discs, characterized by much milder star formation activity, since the adopted star formation time-scale is typically much longer than some dynamical times.[3]

With our prescriptions, large galactic haloes can attain star formation rates of the order of ∼1000 solar masses per year over time-scales of a fraction of Gyr. This is required to explain the submm galaxy population without invoking an extremely top-heavy IMF (e.g. Baugh et al. 2005). In fact, our IMF has the standard Salpeter slope 1.25 in the high-mass tail, and flattens to a slope 0.4 below $1\,\mathrm{M}_\odot$. As shown in Romano et al. (2005), this performs better than the Salpeter one in reproducing the detailed chemical properties of elliptical galaxies.

Star formation promotes the gathering of some cool gas into a low-angular-momentum reservoir around the central supermassive BH. A viable mechanism for this process is the radiation drag (see discussion by Umemura 2001; Kawakatu & Umemura 2002; Kawakatu, Umemura & Mori 2003), which has the nice feature of predicting a mass transfer rate to the reservoir proportional to the SFR to a good approximation:

$$\dot{M}_{\rm RD} = \alpha_{\rm RD} \times 10^{-3}\,(1 - \mathrm{e}^{-\tau_{\rm RD}})\,\psi(t). \tag{16}$$

The constant of proportionality $\alpha_{\rm RD} \sim 1 - 5$ can be fixed to produce a good match to the correlation between the spheroid and the supermassive BH masses observed in the local Universe. The quantity

$$\tau_{\rm RD} \approx \tau_0 \left(\frac{Z}{\mathrm{Z}_\odot}\right) \left(\frac{M_{\rm cold}}{10^{12}\,\mathrm{M}_\odot}\right)^{1/3} \tag{17}$$

represents the effective optical depth of the gas clouds in terms of the normalization parameter $\tau_0 \sim 1$–5 (for more details, see the discussion around equations 14 to 17 in G04).

Eventually, this gas accretes on to the BH powering the nuclear activity; in this early phase, plenty of material is supplied to the BH, so that the latter can accrete close to the Eddington limit

$$\dot{M}_{\rm BH} = \lambda_{\rm Edd}\,\frac{1-\eta}{\eta}\,\frac{M_{\rm BH}}{t_{\rm Edd}}, \tag{18}$$

and grows almost exponentially from a seed of $10^2\,\mathrm{M}_\odot$. The e-folding time involves the Eddington time $t_{\rm Edd} \approx 4 \times 10^8$ yr, the radiative efficiency $\eta \sim 0.15$ and the actual Eddington ratio $\lambda_{\rm Edd} \sim 0.3$– 3.

The energy is fed back to the gas by SN explosions, and BH activity regulates the ongoing star formation and BH growth. The two feedback processes have very different dependencies on halo mass and on galaxy age (e.g. on the time since $z_{\rm f}$). The feedback due to SN explosions removes the star-forming gas at a rate

$$\dot{M}_{\rm SN} = -\frac{2}{3}\,\epsilon_{\rm SN}\,\frac{\eta_{\rm SN}\,E_{\rm SN}}{\sigma^2}\,\psi(t), \tag{19}$$

where σ^2 is the velocity dispersion within the bulge, $E_{\rm SN} \approx 10^{51}$ erg is the energy released in a single SN event, $\eta_{\rm SN}$ is the number of Type II SNe expected per solar mass of formed stars (determined by the IMF) and $\epsilon_{\rm SN} \sim 0.05$ is the fraction of this energy which is effectively coupled to the gas. Thus, the SN feedback evolves almost in parallel with the star formation; it is very effective in low-mass haloes severely limiting the growth of stellar and BH components there, but is of minor importance in the more massive galactic haloes.

The QSO feedback considered by G04 acts both on the cold as well as on the hot gas, unbinding them from the DM halo potential well at a rate

$$\dot{M}_{\rm QSO} \simeq -2 \times 10^3\,\epsilon_{\rm QSO}\,\frac{L_{\rm Edd,46}^{3/2}}{(\sigma/300\,\mathrm{km\,s^{-1}})^2}\,\mathrm{M}_\odot\,\mathrm{yr}^{-1}; \tag{20}$$

this functional form is suggested by theoretical models of line-driven winds and observations of broad absorption line QSOs (see the derivation leading to equations 29 to 31 in G04). The Eddington luminosity $L_{\rm Edd,46}$, in units of 10^{46} erg s^{-1}, is a convenient measure of the BH mass, and $\epsilon_{\rm QSO} \sim 1$–5 is a strength parameter.

As a consequence, the QSO feedback grows exponentially during the early phases of galaxy evolution, following the exponential growth of the supermassive BH mass. It is negligible in the first 0.5 Gyr in all haloes, but abruptly becomes notably important in DM haloes more massive than $10^{12}\,\mathrm{M}_\odot$, structures weakly affected by SN feedback. Eventually, in these systems most of the gas becomes unbound from the potential well of the galaxy halo (see Lapi, Cavaliere & Menci 2005 for the impact of QSO feedback on galaxy groups and clusters), so that star formation and BH activity themselves come to an end on a time-scale which is shorter for more massive galaxies.

Indeed, the positive feedback on BH growth caused by star formation, in cooperation with the immediate and negative feedback of SN, and the abrupt and dramatic effect of QSO feedback are able to reverse the formation sequence of the baryonic component of galaxies compared to that of DM haloes: the star formation and the buildup of central BHs are completed more rapidly in the more massive haloes, thus accounting for the phenomenon now commonly referred to as downsizing.

Before QSO feedback dominates the evolution, radiation is highly obscured by the surrounding dust. In fact, these protogalaxies are extremely faint in the ultraviolet-optical rest frame and are more easily selected at submm wavelengths. The nuclear emission is also heavily obscured, and easier to detect in the hard X-ray band. On the other hand, when the central supermassive BH is massive and powerful enough to remove most of the gas and dust from the surroundings, the active nucleus shines as an optical QSO. Following this stage, the BH is already present at the galaxy centre, thus any subsequent supply of gas to the spheroid produces an immediate QSO feedback, and thus is unable to substantially affect the stellar or BH mass: afterwards, the stellar populations in the spheroid evolve largely in a passive manner.

Other SAMs (e.g. Bower et al. 2006; Croton et al. 2006) introduced the 'radiomode feedback', which is active only in massive objects and at late times to halt cooling flows, but has no effect during the principal growth phase of most galaxies and AGN. Also, the highly idealized pseudo-AGN feedback considered by Hatton et al. (2003) and Cattaneo et al. (2007)[4] is somewhat representative of radiomode feedback. By converse, in G04 a central role is given to the possible feedback originated by the main episode of supermassive BH growth, which is responsible for the QSO activity at high z.

The model described above has proved to be extremely successful in reproducing a wealth of observations, including statistics of submm galaxies, properties of local ellipticals, the results of deep

[3] For instance, $50\,t_{\rm dyn}$ in Hatton et al. (2003), $\sim 200\,t_{\rm dyn}$ in Cole et al. (2000), $\sim 350\,t_{\rm dyn}$ in Bower et al. (2006) and $\sim 15\,t_{\rm dyn}$ in Croton et al. (2006).

[4] They simply stop cooling when $\sum M_{\rm bulge} > 10^{11}\,\mathrm{M}_\odot$, where the sum is over all the galaxies in a halo.

Table 1. Model parameters.

Description	Symbol	Fiducial value	Reference in the text	Impact on this work
Spheroid + BH (ABC)				
Clumping factor	$\mathcal{C}$	7	Equation (13)	Strong
Radiation drag efficiency	$\alpha_{\rm RD}$	2.5	Equation (16)	Mild
Normalization of optical depth	τ_0	1	Equation (17)	Weak
BH radiative efficiency	η	0.15	Equation (18)	Mild
Eddington ratio	$\lambda_{\rm Edd}$	1	Equation (18)	Weak
SN feedback efficiency	$\epsilon_{\rm SN}$	0.05	Equation (19)	Strong
QSO feedback efficiency	$\epsilon_{\rm QSO}$	1.3	Equation (20)	Strong
Disc (vdB01)				
Star formation efficiency	$\epsilon_{\rm sf}$	2.5×10^{-4}	Equation (24)	Strong
Schmidt law exponent	n	1.4	Equation (24)	Mild
Gas velocity dispersion in Toomre	$\sigma_{\rm gas}$	6 km s^{-1}	Equation (26)	Weak
Normalization constant in Toomre	Q	1.5	Equation (26)	Weak
SN feedback efficiency	$\epsilon_{\rm SN}$	10^{-4}	Equation (27)	Strong
Dust (GRASIL)				
Fraction of gas in molecular clouds	$f_{\rm MC}$	0.25	Section 4.3	Mild
Optical depth of molecular clouds (at 1 μm)	$\tau_{\rm MC}$	60	Section 4.3	Weak
Escape time from molecular clouds	$t_{\rm esc}$	2.0 Gyr	Section 4.3	Weak

Note. A Romano IMF $\phi(m_\star)$ is adopted: $\phi(m_\star) \propto m_\star^{-1.25}$ for $m_\star \geq {\rm M}_\odot$ and $\phi(m_\star) \propto m_\star^{-0.4}$ for $m_\star \leq {\rm M}_\odot$.

K-band surveys, demography of supermassive BH relics and statistics of high-redshift QSOs. These successes are essentially inherited by its generalization presented here; in fact, we keep the model parameters fixed to the values used in the papers by Lapi et al. (2006) and Mao et al. (2007). We list the model parameters and their fiducial values in Table 1, stressing their relative relevance in the present context.

3.2 Modelling the disc

At $z < z_{\rm t}$ during the slow accretion phase, conditions become sufficiently quiescent to allow the dissipationless growth of discs from accreting material. Depending on $z_{\rm t}$ and the shape of the individual growth history, under suitable circumstances a substantial disc component may develop. To describe the process, we adopt the model by (van den Bosch 2001, hereafter vdB01); here we provide a quick overview of it, but defer the reader to the original paper for its full description.

At each time-step, new baryons are accreted on to the halo at a rate $f_{\rm b}\,\dot{M}_z$ proportional to the DMs, in terms of the universal baryon to DM fraction $f_{\rm b} \approx 0.17$. As this material enters the halo, it is assumed to be heated to the virial temperature, and to be distributed with an isothermal profile. The angular momentum distribution of the hot gas mirrors that of the DM component, so that the change in the angular momentum over a time interval δt reads

$$\delta J = J(t) - J(t - \delta t), \tag{21}$$

where the halo total angular momentum $J = G\,M^{5/2}\,\lambda/|E|^{1/2}$ is specified in terms of the halo spin parameter λ (see Section 2).

Equating the gained angular momentum to that of a uniformly rotating shell of material, one obtains the circular frequency (see also Fig. 9):

$$\omega_0 = \frac{3}{8\pi}\delta J \left[\int r^4\,\rho(r)\,{\rm d}r\right]^{-1}. \tag{22}$$

The gas is then allowed to cool and collapse, conserving the initial angular momentum gained from the DM halo. The time-scale for condensation $t_{\rm coll} = \max\,(t_{\rm dyn}, t_{\rm cool})$ is given by the maximum of the dynamical and cooling time. After a time $t' = t + t_{\rm coll}$, the cooled gas is added to the disc annuli with radius r_i corresponding to where it becomes centrifugally supported upon dissipationless collapse from the original cylindrical shell radius r_i, i.e.

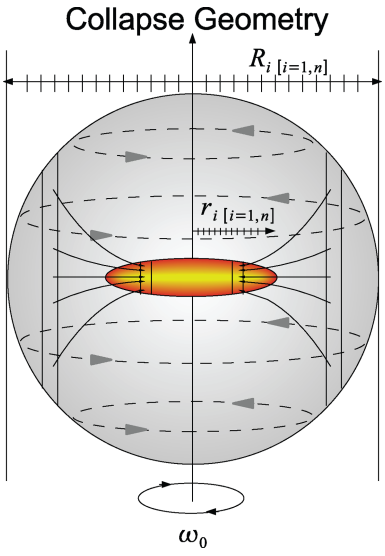

Figure 9. A schematic of the disc formation geometry.

$$R_i = \left[\frac{r_i\,V_{\rm c}(r_i, t')}{\omega_0}\right]^{1/2}, \tag{23}$$

in terms of the local circular velocity $V_{\rm c}(r) \equiv [G\,M(<r)/r]^{1/2}$. Thus, the disc is allowed to grow in an onion-like fashion, and in this computation no specific disc profile is adopted a priori.

The star formation rate is then assumed to follow the empirical Schmidt (1959) law, i.e. it is related to the surface density $\Sigma(r, t)$ of cold gas in the disc through

$$\psi(r, t) = \epsilon_{\rm sf} \left[\frac{\Sigma(r, t)}{{\rm M}_\odot\,{\rm kpc}^{-2}}\right]^n {\rm M}_\odot\,{\rm kpc}^{-2}\,{\rm yr}^{-1}, \tag{24}$$

where $\epsilon_{\rm sf} \sim 2.5 \times 10^{-4}$ is a fudge parameter controlling the star formation efficiency, and $n \sim 1.4$ is fixed to match the properties of local spiral galaxies (Kennicutt 1998).

At each time-step and for each annulus within the disc, we compute the amount of material converted from gas to stars by solving

$$\frac{{\rm d}\Sigma(r,t)}{{\rm d}t} = -\psi(r,t); \tag{25}$$

actually we also impose that a gaseous disc annulus becomes eligible for star formation only once its surface densities surpass a critical threshold $\Sigma_{\rm crit}$ given by the Toomre (1964) criterion:

$$\Sigma_{\rm crit} = \frac{\sigma_{\rm gas}\,\kappa(R)}{3.36\,G\,Q}, \tag{26}$$

where $\kappa(R)$ is the epicycle frequency (see vdB01 for details), $Q \sim 1.5$ is a constant and $\sigma_{\rm gas} \sim 6\ {\rm km\,s^{-1}}$ is the velocity dispersion of the gas.

Cool gas may be removed from the disc through SN winds; we compute the related mass depletion in a way analogous to the spheroidal modelling:

$$\dot{M}_{\rm SN}(r,t) = \frac{2\epsilon_{\rm SN}\,\eta_{\rm SN}\,E_{\rm SN}}{V^2_{\rm esc}(r,t)}\,\psi(r,t), \tag{27}$$

where in the denominator the local escape velocity $V_{\rm esc}$ is used. Finally, we model the chemical evolution of the stellar material on using the instantaneous recycling approximation.

For the sake of coherence, and at variance with vdB01, in the disc modelling we adopt the same IMF used in the treatment of the spheroid evolution. We find that the results concerning the disc structure are affected by 10 per cent from other reasonable choices of the IMF; we may recover reliable matches to the properties of the local galaxy population with all commonly used IMF by altering the fudge parameters of Table 1 within their physical limits.

The main differences in our modelling with respect to vdB01 are the following: we use individual growth history derived from our detailed merger tree, while vdB01 adopts only an averaged smooth fit; we use a the prescription by Macciò et al. (2007) for the concentration parameter of DM haloes, while vdB01 relies on Bullock et al. (2001); finally, at variance with vdB01 we take into account the gravitational effect of the pre-existing spheroid on the dynamics of the forming disc but neglect to model the adiabatic response of the DM haloes to disc settling.

4 RESULTS

4.1 Disc structure and dynamics

In this section, we analyse the behaviour of individual galaxies, focusing on the disc component; the formation and evolution of the spheroidal component have been extensively considered in several previous papers by our team (G04, Cirasuolo et al. 2005; Silva et al. 2005; Lapi et al. 2006).

For this purpose, we select a fiducial model galaxy with current mass $M_0 \approx 5 \times 10^{11}\,{\rm M}_\odot$ similar to that of the Milky Way (see Naab & Ostriker 2006; Xue et al. 2008), and with an average spin parameter $\lambda = 0.04$ (see Macciò et al. 2007). We find that the resulting galaxy components at $z = 0$ are generally in good agreement with observed Milky Way properties, finding that $M_{\rm disc,0} \approx 1.5 \times 10^{10}\,{\rm M}_\odot$ and $M_{\rm bulge,0} \approx 1.3 \times 10^{9}\,{\rm M}_\odot$ (see also Naab & Ostriker 2006).

In Fig. 10, one can see the buildup of the various components for this fiducial galaxy. At $z > z_{\rm t}$, a strong growth of the spheroidal component takes place which is halted by the QSO activity after approximately 10^8 years from $z_{\rm f}$. Following this, the stellar populations in the spheroid evolve passively, and the residual gaseous material is originated from the stellar recycling. At $z < z_{\rm t}$, new gas quiescently accretes on to the halo forming a disc structure; note that star formation is delayed until the cold gas surface density becomes sufficiently large to overcome the critical star formation threshold.

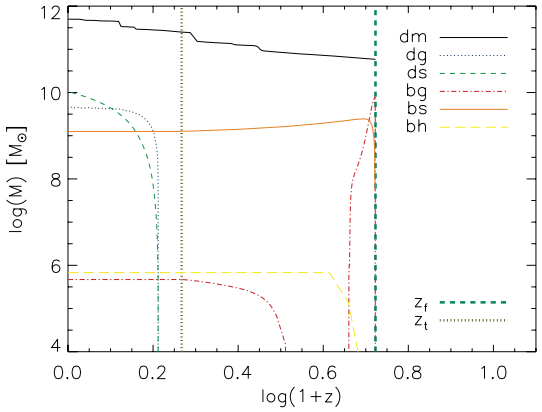

Figure 10. Redshift evolution of the baryonic mass components for a Milky Way sized galaxy at $z = 0$: DM mass (solid/black), disc gas (dotted/blue), disc stars (short-dashed/green), bulge gas (dot–dashed/red) and bulge stars (long-dashed/orange). The two vertical lines mark the transition and formation redshifts.

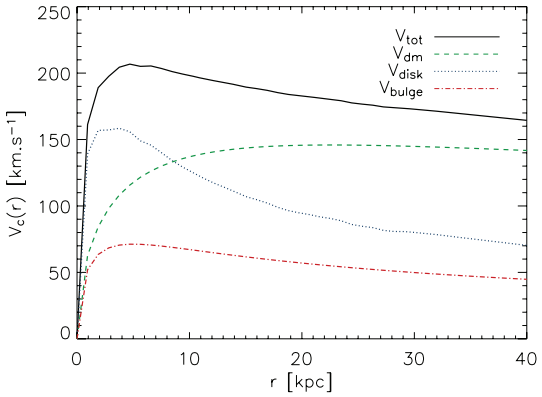

Figure 11. Decomposition of the overall rotation curve (solid line) for our Milky Way type galaxy at $z = 0$ in terms of the contributions from DM (dashed/green line), bulge (dot–dashed/blue line) and disc (dotted/blue line).

In Fig. 11, we present the rotation curve decomposition for our fiducial galaxy. The total rotation curve is flat out to large radii; there it is DM dominated, while in the inner regions the baryonic components of the disc and the bulge dominate the gravitational potential, in agreement with kinematic models of the Milky Way; we find a peak rotation velocity $V_{\rm max} \approx 210\ {\rm km\,s^{-1}}$.

Fig. 12 shows the disc radial surface density profile at $z = 0$; we obtain general exponential stellar profile out to a truncation radius of 16.2 kpc, in broad agreement with the value of 12 kpc observed for the Milky Way (see Naab & Ostriker 2006). The gaseous disc is more extended than the stellar one due to the critical star formation threshold. However, note that the gaseous disc is depleted in the central regions because of star formation, and there the stellar component dominates. Fitting an exponential profile $\Sigma_0\,{\rm e}^{-r/r_{\rm d}}$ to the stellar disc, we find an exponential scale radius $r_{\rm d} \approx 2.6$ kpc, which is comparable to observational estimates 2.5–3.5 kpc for the Milky Way (see Sackett 1997). Finally, within this model, we find a BH

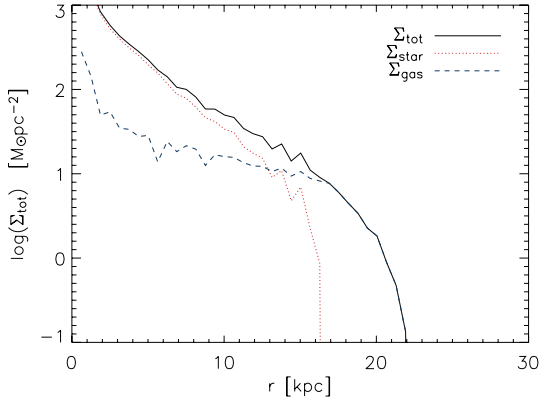

Figure 12. Decomposition of the disc surface density profiles (solid line) for a Milky Way sized galaxy at $z = 0$, in terms of the stellar (dotted line) and gaseous (dashed line) components.

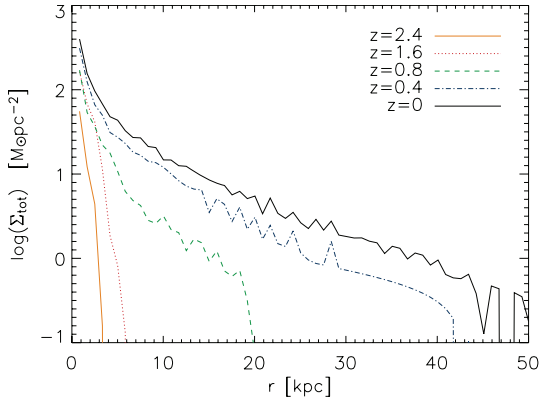

Figure 13. Redshift evolution of the overall surface density profile for a $L_\star$ galaxy with spin parameter $\lambda = 0.06$ resulting in an extension that is twice the fiducial model to highlight the evolution. Note that at $z \approx 0.8$ a minor merger event occurs, the exponential disc structure is temporarily disrupted, and an antitruncated disc (see the text for details) develops.

mass at $z = 0$ of $M_{\rm BH,0} \approx 6.7 \times 10^5\,{\rm M}_\odot$, which is less massive but still consistent with the one at the centre of the Milky Way $M_{\rm BH,0} \approx 3.6 \times 10^6\,{\rm M}_\odot$ (see Eisenhauer et al. 2005).

For the sake of completeness, we highlight the related redshift evolution of the disc profile in Fig. 13. For illustrative purposes, it is clearer to have an elongated disc profile; thus we choose a realization with a spin parameter $\lambda = 0.06$ larger than the fiducial value. The disc (gas and stars) naturally evolves from the inside out, retaining a quasi-exponential profile with scalelength increasing over time. Although the vast majority of model discs have a quasi-exponential surface density profiles, the detailed shape depends on the details of the specific growth history, and in particular on the transition redshift $z_{\rm t}$.

We stress that our discs develop following the buildup of the spheroidal inner component, which affects the overall gravitational potential. Fig. 14 illustrates how the $z = 0$ disc surface density depends on the mass of a pre-existing bulge. We find that for identical realizations for our fiducial model, but imparting a bulge mass by hand, the disc structure (and thus its evolution) is altered. This dynamical interdependence results in a disc structure which becomes significantly more compact as the bulge mass approaches the disc mass at $z = 0$. In addition, we find that with the presence of a substantial spheroid component, higher transition redshifts $z_{\rm t}$ yield more extended discs at $z = 0$.

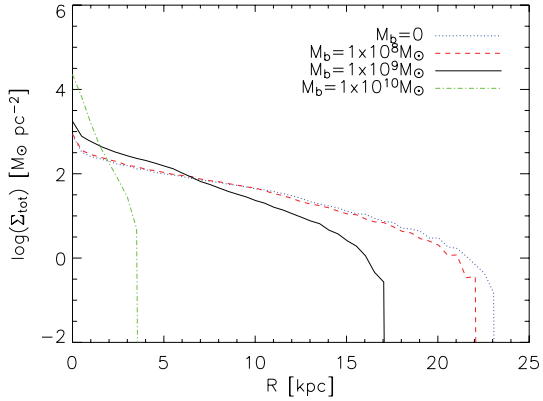

Figure 14. Impact of pre-existing bulge masses on the disc surface density profiles (solid line) for a Milky Way sized galaxy halo $M_0 \approx 5 \times 10^{11}\,{\rm M}_\odot$ at $z = 0$; as the bulge mass approaches the disc mass of about $10^{10}\,{\rm M}_\odot$ discs become more compact. Higher bulge masses yield significantly more concentrated discs.

Recent observational studies have shown that, in general, exponential discs come in three categories, corresponding to simple exponential (type I), truncated (type II) and antitruncated (type III) surface density profiles (Pohlen & Trujillo 2006). We find that exponential surface density profiles (of type I and II) are generated as a generic feature of our model (see Fig. 12). Interestingly, discs which have undergone a recent minor merger event have a significant amount of material added to the outer parts in a non-smooth fashion, and these mimic disc antitruncations (type III; see Fig. 13 at $z \approx 0.8$). However, the disc antitruncations are typically masked through subsequent accretion that restores the overall exponential surface densities. We plan to address this issue in a subsequent work.

4.2 Galaxy properties at $z = 0$

Now we turn to study the properties of the local galaxy population; to this purpose we generate catalogues of galaxies that encompass a representative range of $z = 0$ halo masses, from 10^9 to $10^{14}\,{\rm M}_\odot$ in logarithmic increments. We then exploit the statistics of haloes containing one single galaxy, namely the galaxy halo mass function (GHMF) as provided by Shankar et al. (2006); the latter authors provide the following analytic fit:

$$\Theta(M_0) = \frac{\theta}{\bar{M}} \left(\frac{M_0}{\bar{M}} \right)^{\alpha} {\rm e}^{-M_0/\bar{M}}, \tag{28}$$

with $\alpha \approx 1.84$, $\theta \approx 3.1 \times 10^{-4}\,{\rm Mpc}^{-3}$ and $\bar{M} \approx 1.12 \times 10^{13}\,{\rm M}_\odot$. This function is derived by subtracting the group and cluster mass function (Martinez et al. 2002) from the Sheth & Tormen (2002) mass function. Thus, for haloes with $M_0 <$ a few $10^{13}\,{\rm M}_\odot$ the GHMF closely follows the Sheth & Tormen mass function, while the falloff at larger masses mirrors the increasing probability of multiple occupation. In principle, we may account for the halo occupation number through the full merger tree, but this will introduce uncertainties related to poor knowledge of processes like dynamical friction, tidal stripping, etc.; thus we prefer to bypass this problem using the GHMF.

In Figs 14–16, we compare our model predictions with the results of Shankar et al. (2006) and Baldry, Glazerbrook & Driver (2008), who derive a number of galaxy properties as a function of the host DM halo mass. In Fig. 15, we consider the fraction of stellar to total mass within DM haloes; we see that there is a steep increase in the

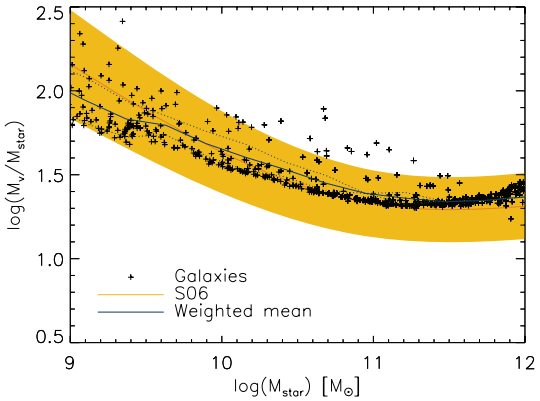

Figure 15. The relation between the host DM halo mass and the stellar mass ratio. Model results (over 1000 realizations) for individual galaxies (crosses), model average (solid line) and quartiles (dashed lines) are compared to the observational determination by Shankar et al. (2006, shaded area).

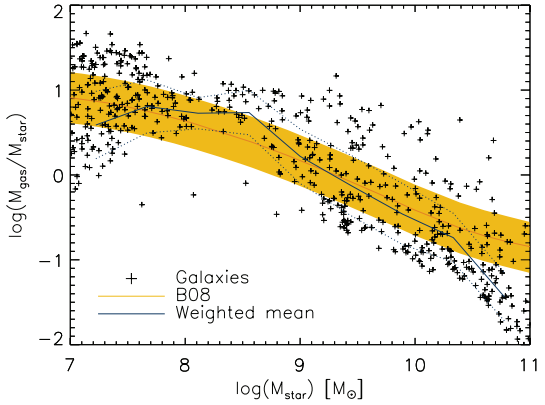

Figure 17. Gas to stellar mass fraction as a function of the stellar mass. Model results (over 1000 realizations) for individual galaxies (crosses), model average (solid line) and quartiles (dashed lines) are compared to the observational determination by Baldry et al. (2008, shaded area).

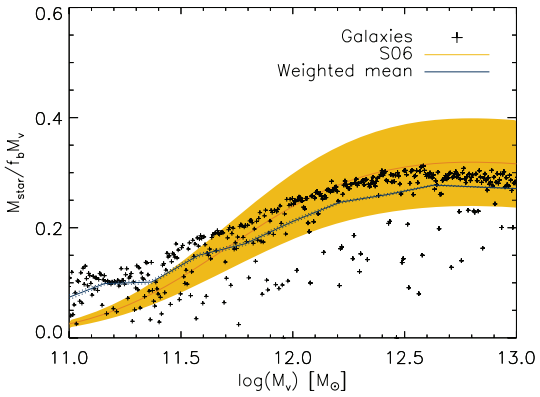

Figure 16. Fraction of baryons converted into stars as a function of host halo mass. Model results (over 1000 realizations) for individual galaxies (crosses), model average (solid line) and quartiles (dashed lines) are compared to the observational determination by Shankar et al. (2006, shaded area).

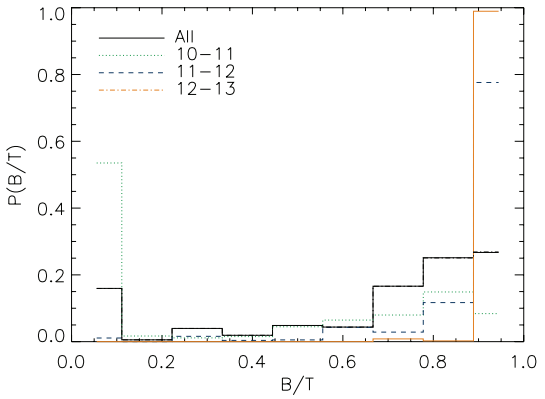

Figure 18. The occurrence of bulge-to-total-mass ratio in our model, binned for different halo mass ranges (results over 1000 realizations); disc-dominated galaxies occur preferentially in low-mass haloes, while spheroid-dominated galaxies occur preferentially in massive haloes.

DM dominance for low-mass haloes, since these provide inefficient environments for star formation mostly due to the impact of SN feedback.

Fig. 16, constituting a different rendition of the previous plot, directly highlights the fraction of available baryons condensed into stars as a function of the host halo mass. In haloes of masses exceeding few $10^{12}\,M_\odot$, star formation is more efficient; in the absence of a substantial impact of QSO feedback, the efficiency would keep growing with increasing mass (despite an increasing difficulty of the cooling processes), while both the data and our model show a clear flattening.

Fig. 17 illustrates the correlation between gas fraction (ratio of the total cold gas to the total baryonic mass within the galaxy) and the overall stellar mass, compared to the data by Baldry et al. (2008); less massive galaxies typically have a significantly larger gas fraction. This is because more massive galaxies are typically spheroid dominated and thus underwent strong gas ejection by the QSO feedback. On the other hand, lower mass galaxies are typically disc dominated, QSO feedback thus is relatively unimportant, and also the critical surface density threshold becomes increasingly difficult to surpass.

Fig. 18 illustrates the occurrence of bulge-to-total-mass ratio in our model, binned in host halo mass. The behaviour of the galaxies in our model is dichotomic, with the disc-dominated galaxies to occur preferentially in low-mass haloes, while spheroid-dominated galaxies to occur preferentially in massive haloes. This result is basically linked to the distribution of transition redshift z_t discussed in Section 2 and illustrated in Fig. 6.

Although not reported here, we stress again that this model inherits from the ABC scenario the good match with the observed local BH mass versus bulge relationships (see G04; Cirasuolo et al. 2005; Lapi et al. 2006).

4.3 Spectrophotometric properties

In order to analyse the luminous properties of galaxies, we interface our model with the spectrophotometric code GRASIL (Silva et al. 1998) that accounts for the attenuation and reradiation of starlight by dust.

GRASIL uses stellar population synthesis models based on the Padova evolutionary tracks, which include the effects of dusty envelopes around asymptotic giant branch stars (Bressan, Granato & Silva 1998). Then, each single stellar population is summed taking into account the appropriate age and metallicity, and weighted with the star formation rate to obtain the unattenuated spectral energy

distribution (SED)

$$F_\lambda(\tau) = \int_0^\tau \zeta_\lambda[\tau - t, Z(t)]\, \psi(t)\, \mathrm{d}t, \qquad (29)$$

where τ is the age of the galaxy, t is the birth age of an individual single stellar population $\zeta_\lambda(t, Z)$ and $\psi(t)$ is the star formation rate.

For the detailed description of dust attenuation and reprocessing of starlight, we defer the reader to the papers by Silva et al. (1998, 2005). We just stress here that GRASIL includes the effect of differential dust extinction of stellar population, i.e. younger stellar generation is more affected by dust obscuration; this is because stars form in molecular clouds, an environment denser than the average, and progressively get rid of them.

The GRASIL SEDs depend on the following basic parameters: the fraction $f_{\rm MC}$ of gas in the form of molecular clouds rather than in the diffuse interstellar medium; the optical depth $\tau_{\rm MC}$ of molecular clouds to the radiation emitted from a source at their centre (at 1 μm); the escape time $t_{\rm esc}$ of newly born stars from molecular clouds. On the basis of previous works in which GRASIL has been coupled with various SAMs, and in particular with the one of the Durham teams (see Granato et al. 2000 for details; also Baugh et al. 2005; Monaco et al. 2007), we set the GRASIL parameters to the standard values reported by Silva et al. (2005) and listed in Table 1. Note that since in this paper we do not consider regions of the SED strongly affected by dust emission, the dependence of our results on these parameters is mild/weak. Due to the preliminary nature of this work, we do not exploit the multiwavelength capabilities of GRASIL to the full extent, but focus on reproducing several local galaxy population properties in selected bands; we delay a more refined analysis for future work.

In Fig. 19, we show the B-band luminosity of our model galaxies as a function of DM halo mass. We find a relatively strong correlation with little scatter, in general agreement with the data by Tonini et al. (2006). The break around 10^{11} $\mathrm{M}_\odot$ is due to the impact of SN feedback in small systems, where star formation becomes progressively less efficient.

Fig. 20 illustrates the I-band Tully–Fisher relation from our model; note that we extract the peak rotation velocity from our model by fitting an exponential to the disc surface density profile. Then, we use the obtained scale radius $r_{\rm d}$ to define the maximum velocity as $V_{\rm max} = V_{\rm c}(2.2\, r_{\rm d})$ in analogy with the observational methods; this procedure therefore does not resort to further assumptions about disc structure and dynamics.

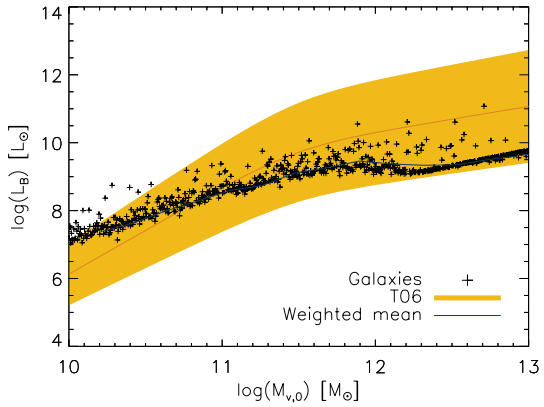

Figure 19. B-band luminosity as a function of the host DM halo mass. Model results (over 1000 realizations) for individual galaxies (crosses), model average (solid line) and quartiles (dashed lines) are compared to the observational determinations collected by Tonini et al. (2006, shaded area).

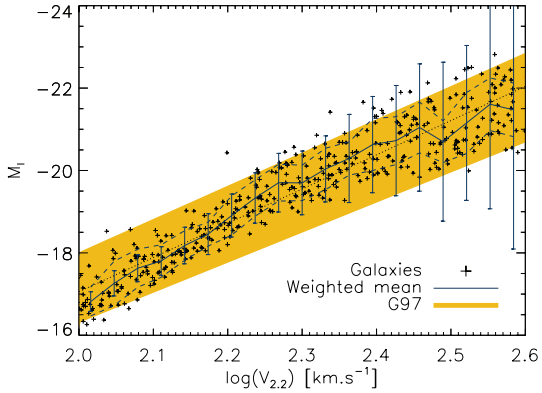

Figure 20. The Tully–Fisher relation. Model results (over 1000 realizations) for individual galaxies (crosses), model average (solid line) and quartiles (dashed lines) are compared to the observational determination by Giovanelli et al. (1997, shaded area). The Possinian error bars illustrate the relative abundance of galaxies with different circular velocities.

Our model result is compared with the data by Giovanelli et al. (1997), finding excellent agreement in both slope and normalization; fitting our result with the law $M_I = m\,[\log_{10}(V_{2.2}) - 2.5] + c$, we obtain $m = -8.30$ and $c = -21.19$, to be compared with the observational values $m = -7.68$ and $c = -21.0$. We also represent the intrinsic scatter in our results by the blue dashed contours, showing a slight if systematic increase in scatter towards higher rotational velocities, in general agreement with observations (Giovanelli et al. 1997). Finally, we show the relative abundances of galaxies as represented by the Poissonian error bars that account for the relative numbers of haloes within a cosmological volume. We see that the slowly rotating, faint galaxies are more abundant; galaxies become rarer as we move towards larger circular velocities, and within our sample we do not find any galaxy with rotational velocities larger than $V_{2.2} > 10^{2.6}$ km s^{-1}.

In Fig. 21, we present the $r^\star$-band luminosity function from our model at $z = 0$, and compare it to the fit by Benson et al. (2007) based on Sloan Digital Sky Survey (SDSS) data; we find an overall good agreement. We confirm, in tune with a number of previous works, that the flattening at the faint end is mainly due to the impact of SN feedback in small systems (Benson et al. 2003 and references therein), and that the steepening at the bright end is mainly caused by the impact of QSO feedback in massive galaxies (Somerville et al. 2008 and references therein). In addition, we highlight the different contributions to the overall luminosity function from the spheroid and the disc component; the latter typically dominates the faint end, while the former dominates the bright end, as expected on an intuitive basis (see also Kauffmann, White & Guiderdoni 1993; Baugh, Cole & Frenk 1996; Kauffmann & Charlot 1998; Somerville & Primack 1999; Hatton et al. 2003; Tasca & White 2005).

We stress that the simultaneous fitting of the galaxy luminosity function and of Tully–Fisher relation is challenging for many SAMs, and so constitutes a big success of our model (see Bell et al. 2003; Courteau et al. 2007; Dutton et al. 2007).

5 DISCUSSION AND CONCLUSIONS

In this paper, we have proposed a novel scenario for the formation and evolution of galaxies in the standard ΛCDM framework.

We have been motivated by several recent high-resolution N-body simulations (Zhao et al. 2003; Diemand et al. 2007; Hoffmann et al.

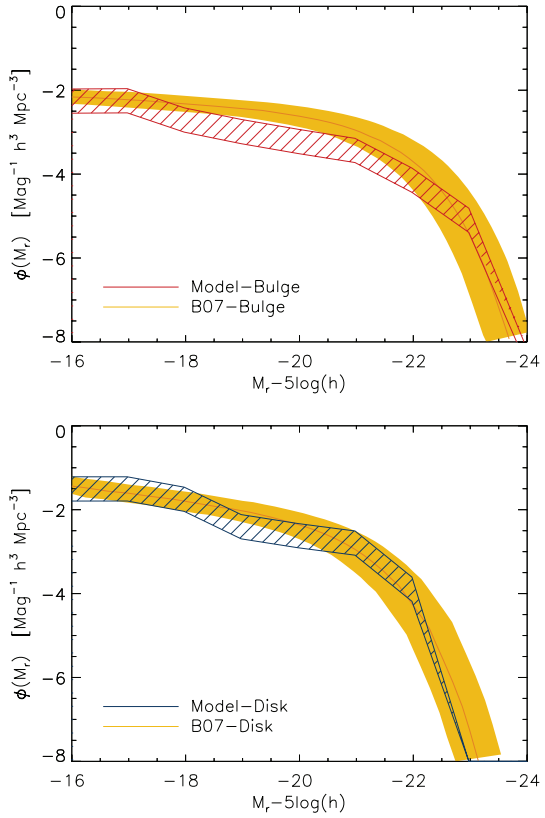

Figure 21. The r^*-band luminosity function. The overall results (over 1000 realizations), with the contributions from spheroids (red hatched region – upper panel) and discs (blue hatched region – lower panel) highlighted, are compared to the fits derived from the SDSS data by Benson et al. (2007, coloured dashed lines).

2007; Ascasibar & Gottloeber 2008) that recognize the DM halo growth to occur in two rather distinct phases: an early violent collapse featuring a few major mergers, and a late quiescent accretion on to the halo outskirts that does not affect the inner regions where the galactic structure resides. We associate these two phases with two different modes of galaxy formation, leading to spheroids and discs.

Specifically, we envisage that spheroids form during the fast collapse phase, when violent major mergers reshuffle the gravitational potential and cause dynamical relaxation and orbit isotropization of the DM and stellar components (see Lapi & Cavaliere 2009). Meanwhile, strong starburst activity and the growth of a central supermassive BH take place in parallel. The ensuing SN explosions and the nuclear activity feed energy back to the baryons, and regulate the ongoing star formation rate and BH growth. These mutual energy feedback actually reverse the formation sequence of the baryonic component of galaxies compared to that of DM haloes: the star formation and the buildup of central BHs are completed more rapidly in the more massive haloes, thus accounting for the phenomenon now commonly referred to as downsizing. In the subsequent slow accretion phase, during which major mergers are rare, the quiescent growth of a disc-like structure around the preformed spheroids can occur by dissipationless collapse.

We then test this new scenario against observations resorting to the semi-analytic technique. To this purpose, we adopt standard and widespread models. As to the DM evolution, we base on the algorithm by Cole et al. (2000) and Parkinson et al. (2008) supplemented by the results of the *N*-body experiments by Zhao et al. (2003). As to the spheroid component, we rely on the prescriptions by G04 and following developments. As to the disc buildup, we base on the recipes by vdB01. Finally, we couple everything to the spectrophotometric code GRASIL by Silva et al. (1998).

Note that the SAM developed here can be viewed as an extension of our previously proposed ABC model (see G04). The latter dealt with the high-redshift spheroid–supermassive-BH formation, and is proven to be successful in many respects (see Cirasuolo et al. 2005; Silva et al. 2005; Lapi et al. 2006; Mao et al. 2007; Lapi et al. 2008). Practically, we now include the disc formation at low redshift, so extending it to encompass all morphological galaxy types and cosmic epochs.

Though we are confident to have described through conceivable physical recipes, the key processes ruling the galaxy formation and evolution, we must admit that our modelling disregards or treats crudely several aspects that may play a relevant role: baryon impacts on the detailed structure of DM haloes, environmental effects, angular momentum evolution, bar instabilities, halo occupation distributions, etc. In fact, in this preliminary study we pursue the strategy of 'keeping it as simple as possible', our aim being to test with minimal ingredients whether our scenario could provide results in accord at least with the local galactic observables, and eventually it proved to perform such a remarkable task surprisingly well.

Specifically, we have shown our model to reproduce the observed stellar mass fractions (see Figs 15 and 16), gas content (see Fig. 17), morphological dichotomy (see Fig. 18), mass-to-light ratios (see Fig. 19), Tully–Fisher relation (see Fig. 20) and luminosity functions (see Fig. 21) of the local galaxy populations. In future works, we aim to compare our model predictions to the intermediate- and high-redshift data; however, note that at $z \gtrsim 2$ our model, built upon the SAM by G04, still performs quite well by construction. We will also pursue the analysis of galaxy statistics at multiple wavelengths; this should allow us to better understand the interplay between the processes involved within our scenario. Finally, we will discuss more extensively the structural properties of the discs emerging from our model, that will constitute test beds for the next generation of SAMs.

ACKNOWLEDGMENTS

We thank an anonymous referee for constructive comments and helpful suggestions. We acknowledge stimulating discussions with L. Silva and A. Schurer. MC has been supported through a Marie Curie studentship from the Sixth Framework Research and Training Network MAGPOP, contract no. MRTN-CT-2004-503929. AL was supported in part by ASI, and thanks INAF-OATS for kind hospitality.

REFERENCES

Ascasibar Y., Gottloeber S., 2008, MNRAS, 386, 2022
Baldry I. K., Glazerbrook K., Driver S. P., 2008, MNRAS, 388, 945
Bardeen J. M., Bond J. R., Kaiser N., Szalay A. S., 1986, ApJ, 304, 15
Barnes J. E., Efstathiou G., 1987, ApJ, 319, 575
Baugh C. M., Cole S., Frenk C. S., 1996, MNRAS, 282, L27
Baugh C. M. et al., 2005, MNRAS, 356, 1191
Bell E. F., McIntosh D. H., Katz N., Weinberg M. D., 2003, ApJS, 149, 289
Bell E. F. et al., 2005, ApJ, 625, 23
Benson A. J. et al., 2003, ApJ, 599, 38
Benson A. J., Danovic D., Frenk C. S., Sharples R., 2007, MNRAS, 379, 841
Blumenthal G., Faber S. M., Flores R., Primack J. R., 1986, ApJ, 301, 27
Bower R. G. et al., 2006, MNRAS, 370, 645

Bressan A., Granato G. L., Silva L., 1998, A&A, 332, 135
Brinchmann J., Ellis R. S., 2000, ApJ, 536, 77
Bullock J. S. et al., 2001, MNRAS, 321, 559
Cattaneo A., Blaizot J., Devriendt J., Guiderdoni B., 2005, MNRAS, 364, 407
Cattaneo A. et al., 2006, MNRAS, 370, 1651
Cattaneo A. et al., 2007, MNRAS, 377, 63
Chiappini C., Matteucci F., Gratton R., 1997, ApJ, 477, 765
Cirasuolo M. et al., 2005, ApJ, 629, 816
Cole S. M., 1991, ApJ, 367, 45
Cole S. M. et al., 1994, MNRAS, 271, 781
Cole S. M., Lacey C. G., Baugh C. M., Frenk C. S., 2000, MNRAS, 319, 168
Courteau S. et al., 2007, ApJ, 671, 203
Cowie L. L., Songaila A., Hu E. M., Cohen J. G., 1996, ApJ, 112, 839
Croton D. J. et al., 2006, MNRAS, 365, 11
Dekel A., Birnboim Y., 2006, MNRAS, 368, 2
Diemand J., Kuhlen M., Madau P., 2007, ApJ, 667, 859
Di Matteo T., Springel V., Hernquist L., 2005, Nat, 433, 604
Driver S. P. et al., 2006, MNRAS, 368, 414
Dutton A. A., van den Bosch F. C., Dekel A., Courteau S., 2007, ApJ, 654, 27
Eisenhauer F. et al., 2005, ApJ, 628, 246
Fontanot F., de Lucia G., Monaco P. L., Somerville R. S., Santini P., 2009, MNRAS, in press (arXiv:0901.1130)
Gavazzi G. et al., 1996, A&A, 312, 397
Giovanelli R. et al., 1997, ApJ, 477, L1
Gnedin O. Y., Kravtsov A. V., Klypin A. A., Nagai D., 2004, ApJ, 616, 16
Granato G. L. et al., 2000, ApJ, 542, 710
Granato G. L. et al., 2004, ApJ, 600, 580 (G04)
Granato G. L. et al., 2006, MNRAS, 368, 72
Guzman R. et al., 1997, ApJ, 489, 559
Hatton S. et al., 2003, MNRAS, 343, 75
Hetznecker H., Burkert A., 2006, MNRAS, 370, 1905
Hoffman Y., Romano-Daz E., Shlosman I., Heller C., 2007, ApJ, 671, 1108
Juneau S. et al., 2005, ApJ, 619, 135
Kauffmann G., Charlot S., 1998, MNRAS, 297, L23
Kauffmann G., White S. D. M., Guiderdoni B., 1993, MNRAS, 264, 201
Kaviraj S., Devriendt J. E. G., Ferreras I., Yi S. K., 2005, MNRAS, 360, 60
Kawakatu N., Umemura M., 2002, MNRAS, 329, 572
Kawakatu N., Umemura M., Mori M., 2003, ApJ, 583, 85
Kennicutt R. C., 1998, ApJ, 498, 541
Khochfar S., Silk J., 2006, ApJ, 648, L21
Kitayama T., Suto Y., 1996, ApJ, 469, 480
Kodama T. et al., 2004, MNRAS, 350, 1005
Kravstov A. V., Klypin A. A., Khokhlov A. M., 1997, ApJS, 111, 73
Lacey C. G., Cole S., 1993, MNRAS, 262, 627
Lapi A., Cavaliere A., 2009, ApJ, 692, 174
Lapi A., Cavaliere A., Menci N., 2005, ApJ, 619, 60
Lapi A. et al., 2006, ApJ, 650, 42
Lapi A. et al., 2008, MNRAS, 386, 608
Li Y., Mo H. J., van den Bosch F. C., Lin W. P., 2007, MNRAS, 379, 689
Lu Y., Mo H. J., Katz N., Weinberg M. D., 2006, MNRAS, 368, 1931
Macciò A. V. et al., 2007, MNRAS, 378, 55
Madau P. et al., 1996, MNRAS, 283, 1388
Madau P., Pozzetti L., Dickinson M., 1998, ApJ, 498, 106
Magorrian J. et al., 1998, AJ, 115, 2285
Mao J. et al., 2007, ApJ, 667, 655
Martinez H. J. et al., 2002, MNRAS, 337, 1441
Mo H. J., Mao S., 2004, MNRAS, 353, 829
Monaco P., Fontanot F., Taffoni G., 2007, MNRAS, 375, 1189
Naab T., Ostriker J. P., 2006, MNRAS, 366, 899
Nagashima M. et al., 2005, MNRAS, 363, L31
Navarro J. F., Frenk C. S., White S. D. M., 1997, ApJ, 490, 493
Noeske K. G. et al., 2007, ApJ, 600, 43
Parkinson H., Cole S., Helly J., 2008, MNRAS, 383, 557
Pohlen M., Trujillo I., 2006, A&A, 454, 759
Portinari L., Chiosi C., 1999, A&A, 350, 827
Rees M. J., Ostriker J. P., 1977, MNRAS, 179, 541
Romano D., Chiappini C., Matteucci F., Tosi M., 2005, A&A, 430, 491
Sackett P. D., 1997, ApJ, 483, 103
Schmidt M., 1959, ApJ, 129, 243
Shankar F. et al., 2006, ApJ, 643, 14
Sheth R. K., Tormen G., 2002, MNRAS, 329, 61
Silk J. S., 1977, ApJ, 211, 638
Silva L., Granato G. L., Bressan A., Danese L., 1998, ApJ, 509, 103
Silva L. et al., 2005, MNRAS, 357, 1295
Somerville R. S., Primack J. R., 1999, MNRAS, 310, 1087
Somerville R. S. et al., 2008, MNRAS, 391, 481
Spergel D. et al., 2007, ApJS, 170, 377
Sugiyama N., 1995, ApJS, 100, 281
Swinbank A. M. et al., 2008, MNRAS, 391, 420
Tasca L. A. M., White S. D. M., 2005, MNRAS, submitted (astro-ph/0507249)
Taylor J. E., Navarro J. F., 2001, ApJ, 563, 483
Thomas D., Maraston C., Bender R., Mendes de Oliveira C., 2005, ApJ, 621, 673
Tonini C., Lapi A., Shankar F., Salucci P., 2006, ApJ, 638, L13
Toomre A., 1964, ApJ, 139, 1217
Umemura M., 2001, ApJ, 560, L29
van den Bosch F. C., 2001, MNRAS, 327, 1334 (vdB01)
Vitvitska M. et al., 2002, ApJ, 581, 799
Wechsler R. H. et al., 2002, ApJ, 568, 52
White S. D. M., Rees M. J., 1978, MNRAS, 183, 341
Xue X. X. et al., 2008, ApJ, 684, 1143
Zavala J., Okamoto T., Frenk C. S., 2008, MNRAS, 387, 364
Zhao D. H., Mo H. J., Jing Y. P., Börner G., 2003, MNRAS, 339, 12

This paper has been typeset from a TEX/LATEX file prepared by the author.